Bol. Soc. Paran. Mat.
©SPM – E-ISSN-2175-1188
SPM: www.spm.uem.br/bspm

(3s.) **v. 2025 (43)** : 1–11.
ISSN-0037-8712
doi:10.5269/bspm.77563

Investigation of inelastic power-law model under thermal conditions by using a developed method

Samah H. Al-Zaidi and Anas Al-Haboobi*

ABSTRACT: This study extends the developed Taylor-Galerkin/Pressure-Correction (DTG/PC) method to simulate the behavior of inelastic, incompressible fluids under thermal conditions, utilizing a power-law model to characterize the fluid's viscosity. The approach is grounded in the Taylor-Galerkin/Pressure-Correction finite element framework (TG/PC), wherein the energy equation is coupled with the incompressible Navier - Stokes equations to simultaneously capture fluid motion and thermal transport. The novelty of this research lies in the development of a highly accurate method to analyze inelastic fluid under thermal conditions. The finite element method utilizing the (TG/PC) framework has been enhanced through the integration of novel stages specifically designed to directly solve the equation of energy. A significant advancement in this refinement process was the implementation of the two-step Lax-Wendroff numerical scheme to the energy equation. This modification introduced two supplementary computational steps dedicated to energy-related calculations within the existing (TG/PC) algorithmic structure. The accuracy and reliability of the numerical method were assessed by examining the effects of the power-law index (n) and the consistency coefficient (m) on velocity, pressure, temperature, shear stress, and normal stress. The numerical results showed excellent agreement with established physical principles and previous studies, underscoring the method's validity and effectiveness.

Key Words: Channel flow, viscosity, Thermal flow, Incompressible flow, Non-Newtonian, inelastic flow, Power-law model.

Contents

1. Introduction

Non-Newtonian fluids are characterized by a viscosity that varies with the applied stress or shear rate, in contrast to Newtonian fluids, where viscosity remains constant. Thermal fluids, by comparison, are utilized in heat transfer processes. The interaction between these two fluid types is of considerable importance, as the flow behavior of non-Newtonian fluids can significantly influence heat transfer rates. Consequently, researchers focus on studying the combined behavior of non-Newtonian and thermal fluids to enhance understanding of their performance under varying thermal conditions, which can lead to advancements in industrial processes [16,14,15]. Given the importance of this topic, numerous researchers have conducted extensive studies and employed various numerical methods. For an overview of this body of research, refer to [17,18,19,20,21]. The TG/PC method, primarily based on the finite element method (FEM), is one of the most effective and accurate numerical methods for addressing prominent fluid-related challenges. Initially introduced by Townsend and Webster [22], this method has been widely applied to solve various fluid-related problems, predominantly under isothermal conditions. For examples of such

* Corresponding author.
2010 *Mathematics Subject Classification:* 35Q30, 76M10, 80Axx.
Submitted June 29, 2025. Published September 01, 2025

research, see references [23,24,25,26,11,27,29].
In 2023, Al-Haboobi and Al-Muslimawi introduced a numerical method for addressing fluid flow problems under non-isothermal conditions, as presented in two publications. The first study focused on incompressible Newtonian flow [10], while the second extended the approach to compressible Newtonian flow [12]. The present work marks a notable advancement, as it is the first to apply this numerical technique to non-isothermal inelastic (non-Newtonian) flow problems. Building upon their earlier work, this study extends the method to address more complex scenarios involving unsteady thermal conditions. Specifically, it investigates the behavior of inelastic fluids, whose viscous shear stress is governed by a power-law constitutive model. This formulation effectively describes both shear-thinning and shear-thickening phenomena in such fluids. The power-law model, originally formulated by Ostwald and de Waele [28], is employed in this study to characterize the shear-dependent viscosity of non-Newtonian fluids. This constitutive relation effectively captures the essential rheological behavior by correlating the apparent viscosity to the local shear rate. Power-law fluids serve as simplified yet robust representations of complex fluids in numerous chemical and industrial processes, including polymer extrusion, food processing, slurry transport, and various biological systems, where shear-thinning or shear-thickening behavior is prevalent. In this work, the flow dynamics of power-law fluids are examined within an axisymmetric channel under non-isothermal conditions. The analysis encompasses a wide spectrum of physical parameters, including power-law index (n) and consistency parameter (m). The primary objective is to examine the effects of these two parameters on velocity (v), pressure (p), temperature (T), shear stress (τ_{rz}), and normal stress (τ_{zz}). The findings demonstrate that the newly developed method offers significant potential for advancing the study of non-Newtonian fluid dynamics under thermal conditions. Its exceptional effectiveness enhances our understanding of these systems and provides a powerful tool for addressing complex and challenging problems in the field.

2. Mathematical Description

The continuity, momentum and energy equations that govern the thermal incompressible inelastic flow are expressed in two dimension cylindrical coordinates (r, z), respectively, as [10,9]:

$$\nabla \cdot \mathrm{v} = 0, \tag{2.1}$$

$$\rho\left(\frac{\partial \mathrm{v}}{\partial t} + (\mathrm{v}\cdot\nabla)\mathrm{v}\right) = \nabla^2(\mu_s \mathrm{v}) - \nabla p, \tag{2.2}$$

$$\rho C_p\left(\frac{\partial T}{\partial t} + (\mathrm{v}\cdot\nabla)T\right) = \alpha\nabla^2 T + \phi. \tag{2.3}$$

In component form

$$\frac{1}{r}\frac{\partial}{\partial r}(r\mathrm{v}_r) + \frac{\partial}{\partial z}(\mathrm{v}_z) = 0, \tag{2.4}$$

$$\rho\left(\frac{\partial \mathrm{v}_r}{\partial t} + \mathrm{v}_r\frac{\partial \mathrm{v}_r}{\partial r} + \mathrm{v}_z\frac{\partial \mathrm{v}_r}{\partial z}\right) = \left(\frac{1}{r}\frac{\partial}{\partial r}\left(\mu_s r\frac{\partial \mathrm{v}_r}{\partial r}\right) - \frac{\mathrm{v}_r}{r^2} + \frac{\partial^2 \mathrm{v}_r}{\partial z^2}\right) - \frac{\partial p}{\partial r}, \tag{2.5}$$

$$\rho\left(\frac{\partial \mathrm{v}_z}{\partial t} + \mathrm{v}_r\frac{\partial \mathrm{v}_z}{\partial r} + \mathrm{v}_z\frac{\partial \mathrm{v}_z}{\partial z}\right) = \left(\frac{1}{r}\frac{\partial}{\partial r}\left(\mu_s r\frac{\partial \mathrm{v}_z}{\partial r}\right) + \frac{\partial^2 \mathrm{v}_z}{\partial z^2}\right) - \frac{\partial p}{\partial z}, \tag{2.6}$$

$$\rho C_p\left(\frac{\partial T}{\partial t} + \mathrm{v}_r\frac{\partial T}{\partial r} + \mathrm{v}_z\frac{\partial T}{\partial z}\right) = \alpha\left(\frac{1}{r}\frac{\partial}{\partial r}(r\frac{\partial T}{\partial r}) + \frac{\partial^2 T}{\partial z^2}\right) + \phi. \tag{2.7}$$

In this context, $\mathrm{v} = (\mathrm{v}_r, \mathrm{v}_z)$ represents the velocity vector, while p, ρ and μ_s denote the pressure, density, and solvent viscosity of the fluid, respectively. Additionally, T corresponds to the temperature of the fluid, C_p signifies the specific heat capacity α istands for the thermal conductivity, and ϕ is a dissipation function.
The solvent viscosity is calculated using a power-law model, which is defined as [11]:

$$\mu_s = m(\gamma)^{n-1}. \tag{2.8}$$

Where, m is consistency parameter, n is power-law index and γ represent shear rate of simple shear flow defined as [11]:

$$\gamma = 2\sqrt{II}. \tag{2.9}$$

In this formulation, II represents the second invariant of the rate of strain tensor. For an axisymmetric coordinate system, this invariant can be expressed in the following form [11]:

$$II = \frac{1}{2}\left\{\left(\frac{\partial \mathrm{v}_r}{\partial r}\right)^2 + \left(\frac{\partial \mathrm{v}_z}{\partial z}\right)^2 + \left(\frac{\mathrm{v}_r}{r}^2\right) + \frac{1}{2}\left(\frac{\partial \mathrm{v}_r}{\partial r} + \frac{\partial \mathrm{v}_z}{\partial z}\right)^2\right\}. \tag{2.10}$$

To non-dimensionalize the conservation (of mass, momentum and energy), we have used the following variables:

$t^* = \dfrac{t}{L/V_\infty}$, $\mathrm{v}^* = \dfrac{\mathrm{v}}{V_\infty}$, $p^* = \dfrac{p - p_\infty}{\rho V_\infty^2}$, $T^* = \dfrac{T - T_\infty}{\Delta T}$,

here, V_∞ denotes the characteristic velocity, p_∞ represents the characteristic pressure, and T_∞ signifies the characteristic temperature. Additionally, L corresponds to the characteristic length, while ΔT defines a temperature difference.

Using above transformations, the following non-dimensional form of the conservation (of mass, momentum and energy) are,

$$\nabla \cdot \mathrm{v} = 0, \tag{2.11}$$

$$Re\left(\frac{\partial \mathrm{v}}{\partial t} + (\mathrm{v}\cdot\nabla)\mathrm{v}\right) = \nabla^2(\mu_s \mathrm{v}) - \nabla p, \tag{2.12}$$

$$RePr\left(\frac{\partial T}{\partial t} + (\mathrm{v}\cdot\nabla)T\right) = \nabla^2 T + PrEc\phi. \tag{2.13}$$

In component form

$$\frac{1}{r}\frac{\partial}{\partial r}(r\mathrm{v}_r) + \frac{\partial}{\partial z}(\mathrm{v}_z) = 0, \tag{2.14}$$

$$Re\left(\frac{\partial \mathrm{v}_r}{\partial t} + \mathrm{v}_r\frac{\partial \mathrm{v}_r}{\partial r} + \mathrm{v}_z\frac{\partial \mathrm{v}_r}{\partial z}\right) = \left(\frac{1}{r}\frac{\partial}{\partial r}\left(\mu_s r\frac{\partial \mathrm{v}_r}{\partial r}\right) - \frac{\mathrm{v}_r}{r^2} + \frac{\partial^2 \mathrm{v}_r}{\partial z^2}\right) - \frac{\partial p}{\partial r}, \tag{2.15}$$

$$Re\left(\frac{\partial \mathrm{v}_z}{\partial t} + \mathrm{v}_r\frac{\partial \mathrm{v}_z}{\partial r} + \mathrm{v}_z\frac{\partial \mathrm{v}_z}{\partial z}\right) = \left(\frac{1}{r}\frac{\partial}{\partial r}\left(\mu_s r\frac{\partial \mathrm{v}_z}{\partial r}\right) + \frac{\partial^2 \mathrm{v}_z}{\partial z^2}\right) - \frac{\partial p}{\partial z}, \tag{2.16}$$

$$RePr\left(\frac{\partial T}{\partial t} + \mathrm{v}_r\frac{\partial T}{\partial r} + \mathrm{v}_z\frac{\partial T}{\partial z}\right) = \left(\frac{1}{r}\frac{\partial}{\partial r}(r\frac{\partial T}{\partial r}) + \frac{\partial^2 T}{\partial z^2}\right) + PrEc\phi. \tag{2.17}$$

Where Re, Pr and Ec are non-dimensional values representing the Reynolds, Prandtl, and Eckert numbers, respectively, defined as [10,12]:

$$Re = \frac{\rho V_\infty L}{\mu_s},$$

$$Pr = \frac{\mu_s}{\alpha/C_p},$$

$$Ec = \frac{V_\infty^2}{C_p \Delta t}.$$

3. Numerical Algorithm

The (DTG/PC) algorithm employs a fractional-step approach comprising six phases. In the first three phases, the intermediate velocity ($\mathrm{v}^{n+1/2}$), (v^*) and temperature ($T^{n+1/2}$) components are computed using a two-step predictor-corrector scheme, starting from the initial velocity, temperature, and pressure fields. In the fourth phase, the updated temperature (T^{n+1}) is calculated using $\mathrm{v}^{n+1/2}$ and $T^{n+1/2}$. The fifth phase involves evaluating the pressure difference ($q = p^{n+1} - p^n$) based on v^*, with the Cholesky method applied to solve the resulting system. Finally, in the sixth phase, the velocity field (v^{n+1}) is determined using the pressure difference (q) and v^* through Jacobi iteration.
Then the fractional step can be written as:

$$\text{stage 1}: \quad \mathrm{v}^{n+1/2} = \mathrm{v}^n + \frac{\Delta t}{2Re}(Ł(\mathrm{v}^n) - \nabla p^n), \tag{3.1}$$

$$\text{stage 2}: \quad T^{n+1/2} = T^n + \frac{\Delta t}{2RePr}Ģ(\mathrm{v}^n, T^n), \tag{3.2}$$

$$\text{stage 3}: \quad \mathrm{v}^* = \mathrm{v}^n + \frac{\Delta t}{Re}(Ł(\mathrm{v}^{n+1/2}) - \nabla p^n), \tag{3.3}$$

$$\text{stage 4}: \quad T^{n+1} = T^n + \frac{\Delta t}{RePr}Ģ(v^{n+1/2}, T^{n+1/2}), \tag{3.4}$$

$$\text{stage 5}: \quad \nabla^2 q^{n+1} = \frac{Re}{\vartheta \Delta t}\nabla \cdot \mathrm{v}^*, \tag{3.5}$$

$$\text{stage 6}: \quad \mathrm{v}^{n+1} = \mathrm{v}^* - \frac{\vartheta \Delta t}{Re}\nabla q^{n+1}. \tag{3.6}$$

Where,

$$Ł(\mathrm{v}) = \nabla^2(\mu_s \mathrm{v}) - Re(\mathrm{v} \cdot \nabla)v,$$

$$Ģ(\mathrm{v}, T) = \nabla^2 T - RePr(\mathrm{v} \cdot \nabla)T + PrEc\phi.$$

Additionally, for $\vartheta \in [0, 1]$, selecting $\vartheta = \frac{1}{2}$ corresponds to the widely used Crank - Nicolson scheme, a second-order temporal discretization method. This choice is commonly referred to as the Crank - Nicolson parameter see [13]. Viscosity is calculated using the relationship presented in Eq.2.8. For a detailed derivation of the six stages of the developed method, readers are referred to the original source [10]. The stages can be represented in matrix form as follows:

$$\text{stage 1}: \quad \frac{2Re}{\Delta t}\mathfrak{M}\Delta V^{n+1/2} = \mathfrak{L}^\dagger P^n - \mathfrak{D}V^n - Re\mathfrak{N}(V^n)V^n + \mathfrak{B}, \tag{3.7}$$

$$\text{stage 2}: \quad \frac{2RePr}{\Delta t}\mathfrak{M}\Delta T^{n+1/2} = -RePr(\mathfrak{N}(T^n)V^n) - \mathfrak{D}T^n + \mathfrak{B} + \Phi, \tag{3.8}$$

$$\text{stage 3}: \quad \frac{Re}{\Delta t}\mathfrak{M}\Delta V^* = \mathfrak{L}^T P^n - \mathfrak{D}V^{n+1/2} - Re\mathfrak{N}(V^{n+1/2})V^{n+1/2} + \mathfrak{B}, \tag{3.9}$$

$$\text{stage 4}: \quad \frac{RePr}{\Delta t}\mathfrak{M}\Delta T^{n+1} = -RePr(\mathfrak{N}(T^{n+1/2})V^{n+1/2}) - \mathfrak{D}T^{n+1/2} + \mathfrak{B} + \Phi, \tag{3.10}$$

$$\text{stage 5}: \quad \mathfrak{K}\mathfrak{Q}^{n+1} = -\frac{Re}{\vartheta \Delta t}\mathfrak{L}V^*, \tag{3.11}$$

$$\text{stage 6}: \quad \frac{Re}{\Delta t}\mathfrak{M}\Delta V^{n+1} = \vartheta \mathfrak{L}^T \mathfrak{Q}^{n+1}, \tag{3.12}$$

where, $\Delta V^{n+1/2} = V^{n+1/2} - V^n$, $\Delta V^{n+1} = V^{n+1} - V^*$, $\Delta T^{n+1/2} = T^{n+1/2} - T^n$, $\Delta T^{n+1} = T^{n+1} - T^n$ and $\Delta V^* = V^* - V^n$. V, T, and P are represent velocity, temperature, and pressure vectors, respectively. The vector of pressure difference defined as $\mathfrak{Q}^{n+1} = P^{n+1} - P^n$.
Below we review the structure and notation of the matrix as follows:

$$\mathfrak{M}_{ij} = [\Lambda_i, \Lambda_j] = \int_\Omega \Lambda_i \cdot \Lambda_j \, d\Omega, \quad \mathfrak{L}_{ij} = (\gamma_i, \nabla \cdot \Lambda_j) = \int_\Omega \gamma_i \nabla . \Lambda_j \, d\Omega,$$

$$\mathfrak{D}_{ij} = [\nabla\Lambda_i, \nabla\Lambda_j] = \int_\Omega \mu_s \nabla\Lambda_i \cdot \nabla\Lambda_j \, d\Omega, \quad \mathfrak{K}_{ij} = [\nabla\Upsilon_i, \nabla\Upsilon_j] = \int_\Omega \nabla\,\Upsilon_i \cdot \nabla\,\Upsilon_j \; d\Omega,$$

$$\mathfrak{N}(V)_{ij} = [\Lambda_i, \mathrm{v}\cdot\nabla\Lambda_j] = \int_\Omega \left(\sum_l \Lambda_i\Lambda_j V^l \cdot \nabla\right) \Lambda_j \, d\Omega,$$

$$\mathfrak{N}(T)_{ij} = [\Lambda_i, T\cdot\nabla\Lambda_j] = \int_\Omega \left(\sum_l \Lambda_i\Lambda_j T^l \cdot \nabla\right) \Lambda_j \, d\Omega,$$

$$\mathfrak{B}_i = [\Lambda_i, g]_\Gamma = \int_\Gamma g\cdot\Lambda_i \, d\Gamma \ ,$$

in this formulation, $\mathfrak{B}$ epresents a vector corresponding to the natural boundary conditions, while g denotes a specified function.

4. Specification of the Problem

In this study, we examine inelastic Poiseuille flow (Ps) through a straight, axisymmetric channel in two dimensions ($2D$) under non-isothermal conditions. A detailed triangular finite element mesh, illustrated in Fig.1, is employed, featuring a refined junction structure. The mesh is characterized by a total of $6,669$ elements, $3,630$ vertices, and $14,520$ degrees of freedom.

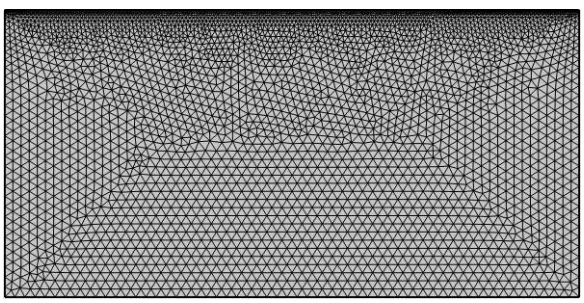

Figure 1: Structured finite element mesh.

The boundary conditions necessary to solve the problem are depicted in Fig.2

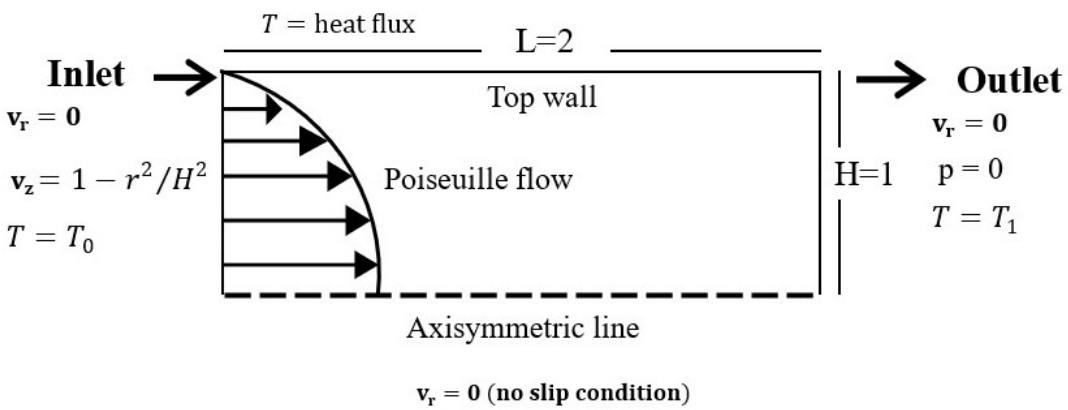

Figure 2: The flow problem's geometry boundary conditions.

5. Results and Discussions

In this study, we applied a numerical investigation using DTG/PC for solving the problem under consideration. The effect of the power-law index (n) and the consistency parameter (m) on various variables and parameters is examined.

n-variation: The power-law index (n) plays a pivotal role in defining the flow dynamics of non-Newtonian fluids. In contrast to Newtonian fluids, which maintain a constant viscosity, non-Newtonian fluids display viscosity that varies depending on the shear rate-the measure of fluid deformation over time [1]. In this study, we investigate the impact of varying the power-law index n at values $n = 0.4, 0.8, 1, 1.4$, and 1.8, while keeping all other parameters constant ($Re = Pr = m = 1$). Figure 3 illustrates the influence of n on both axial velocity (v) and pressure (p). When $n = 1$, the fluid exhibits Newtonian behavior; for $n < 1$ or $n > 1$, the fluid displays non-Newtonian characteristics. The profiles reveal that both velocity and pressure increase as n rises, reaching their highest levels in the shear-thickening regime. Specifically, the maximum velocity occurs in the shear-thickening region, reaching approximately 1.13 units at $n = 1.8$. Similarly, the highest pressure levels are also observed in the shear-thickening regime. These results align with the known physical properties of non-Newtonian fluids. As n decreases, the fluid's viscosity increases, causing greater resistance to flow. This, in turn, leads to higher velocity and pressure levels under the same flow conditions [7].

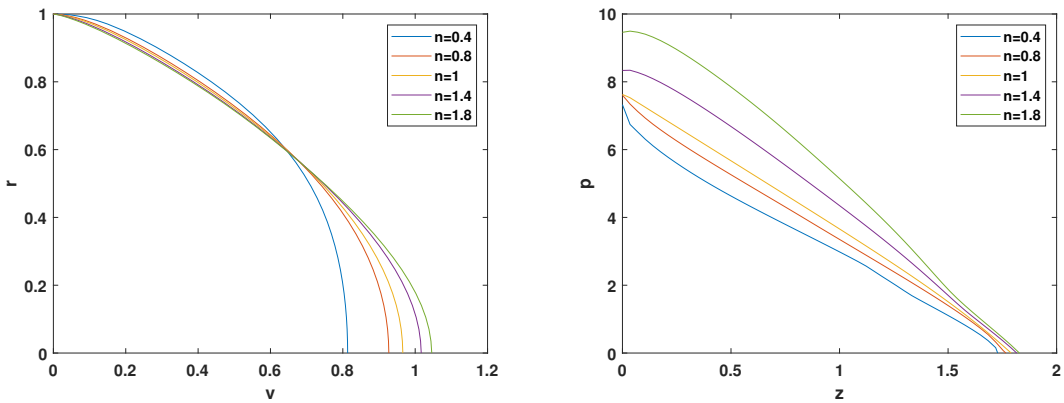

Figure 3: Influence of variation n on axial velocity and pressure.

For the temperature T, an increase n leads to greater resistance to flow within the fluid, thereby intensifying temperature gradients. As a result, the difference between the wall temperature and the bulk fluid temperature becomes more pronounced. This effect is due to the increased resistance to flow in shear-thickening fluids (higher n), which contributes to steeper temperature gradients, as illustrated in Fig.4.

The viscosity (μ_s) is directly correlated with the shear rate (γ), as illustrated in Eq.(2.8). Fig.5 depicts the influence of n on this relationship, revealing three distinct cases based on the value of n. For $n < 1$, the fluid exhibits shear-thinning behavior, where shear rate increases with decreasing viscosity. This effect is attributed to the presence of polymers within the fluid, which can become entangled with each other. At higher shear rates, these entanglements are stretched and disentangled, enabling the molecules to flow more freely and reducing the overall viscosity. Conversely, when $n > 1$, viscosity increases as shear rate rises, indicating shear-thickening behavior. Finally, for $n = 1$, the fluid exhibits Newtonian characteristics, maintaining a constant viscosity irrespective of shear rate. For further details, refer to [2].

Finally, we examine the effect of n on both shear stress (τ_{rz}) and normal stress (τ_{zz}) as shown in Fig. 6. It is observed that as n increases, both shear and normal stresses also increase in magnitude, attributable to the shear-thickening behavior of the fluid. Everything that has been mentioned up until this point is consistent with what was provided in [1,3,5,4].

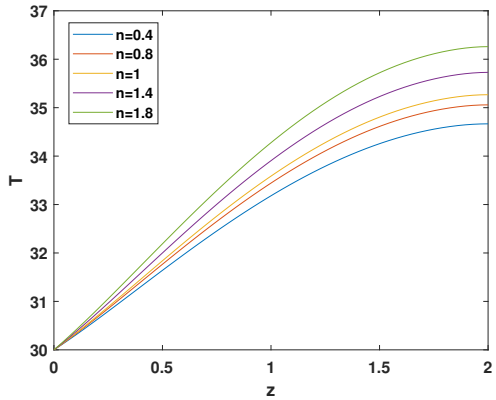

Figure 4: Influence of variation n on temperature.

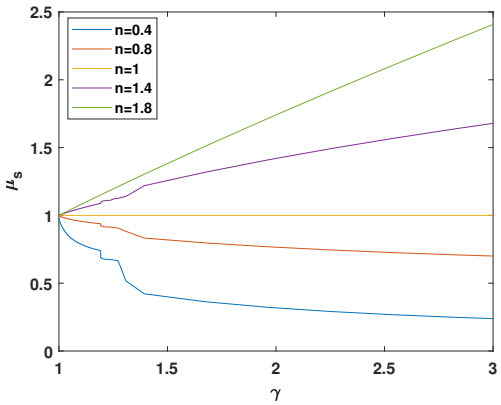

Figure 5: Influence of variation n on relation between viscosity & shear rate .

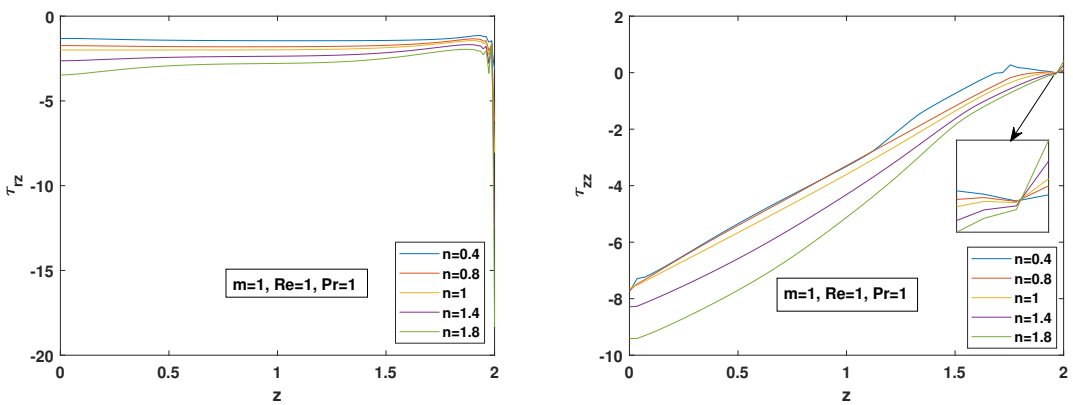

Figure 6: Influence of variation n on axial shear stress and normal stress.

m-variation: The consistency parameter (m) measures a non-Newtonian fluid's average viscosity, describing its response to varying shear rates and its resistance to deformation [6]. We examine the effects of varying the consistency parameter m at values $5, 10, 20$ and 50, in both shear-thinning ($n = 0.8$) and shear-thickening ($n = 1.8$) while holding all other parameters constant ($Re = Pr = 1$). Fig.7

demonstrates that the impact of increasing the consistency parameter (m) on the velocity profile is negligible. However, upon closer observation, a slight increase in the velocity level can be detected as m increases, indicating a minimal yet measurable effect. As shown in Fig.7, the impact is less pronounced for $n = 0.8$ and more substantial for $n = 1.8$, reflecting the characteristics of shear-thinning and shear-thickening behaviors, respectively.

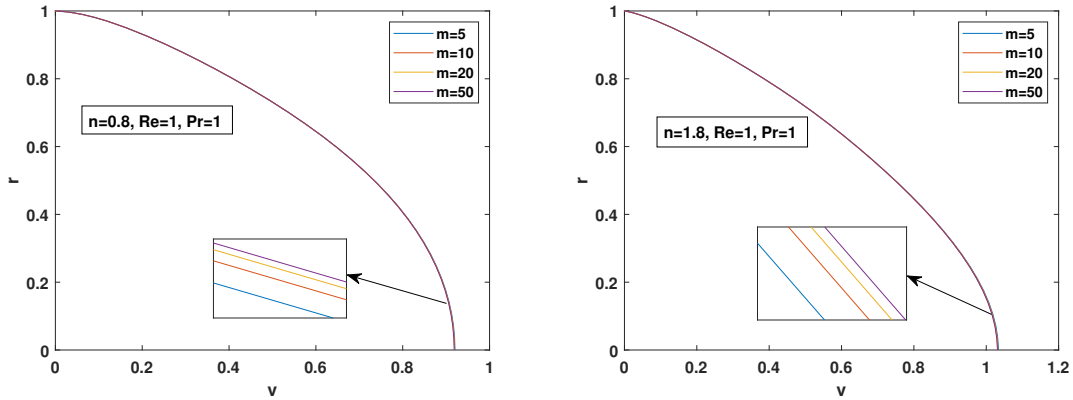

Figure 7: Influence of variation m on axial velocity.

For pressure, an increase in m necessitates a corresponding increase in p to maintain the same flow rate. As the fluid's resistance to flow rises, a greater driving force (pressure) is required to sustain the original velocity profile. This effect is more pronounced when $n > 1$, as illustrated in Fig.8. All the above results align with the findings presented in [7]. The effect on temperature is illustrated in Fig.9, where

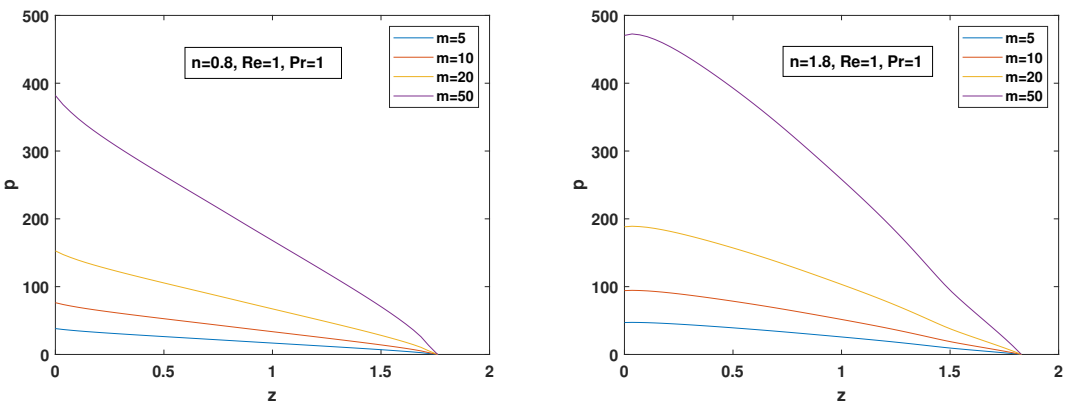

Figure 8: Influence of variation m on pressure drop.

increasing m leads to a marked rise in temperature. This increase is more pronounced for $n = 1.8$ (shear-thickening), as higher values of m correspond to greater viscosity. Consequently, the fluid experiences increased internal friction, which results in higher localized temperatures due to viscous heating. The results are in good agreement with the reported values in [8].

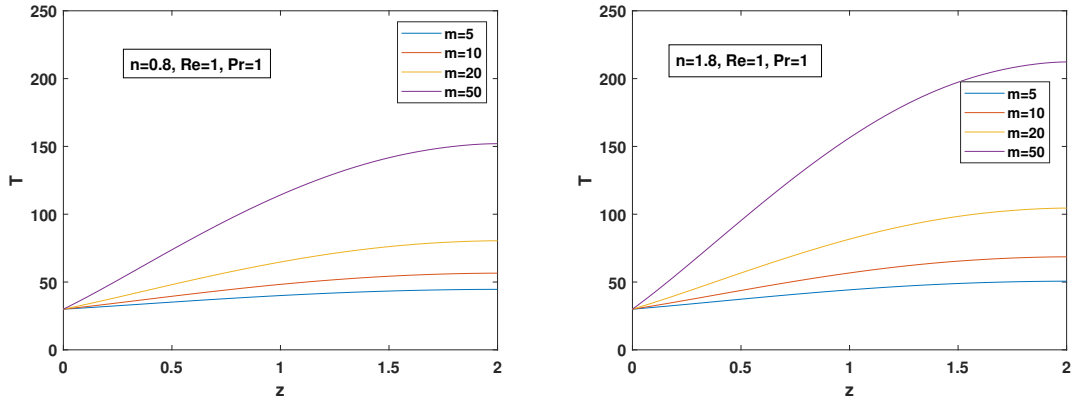

Figure 9: Influence of variation m on temperature.

Finally, we analyze the impact of m on both shear stress τ_{rz} and normal stress τ_{zz}. The results, presented in Figs.10 and 11, demonstrate that increasing m leads to a rise in the magnitude of both τ_{rz} and τ_{zz}, particularly in shear-thickening fluids. This behavior is attributed to the increased viscosity associated with higher values of m see [6].

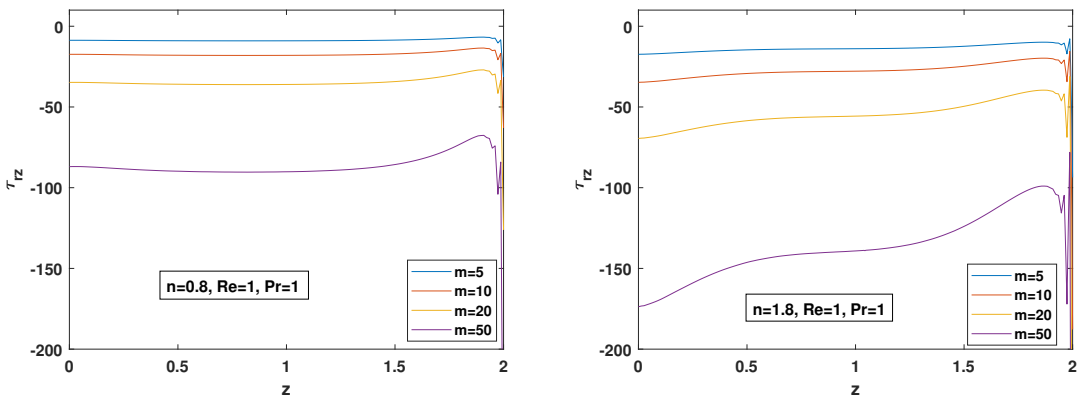

Figure 10: Influence of variation m on axial shear stress.

6. Conclusions

We simulated incompressible and inelastic flow under non-isothermal conditions using the DTG/PC method in a system of cylindrical coordinates. The key objective of this study is the effectiveness and reliability of the developed numerical method by studying the effect of power law index (n) and consistency coefficient (m) on axial velocity, pressure drop, temperature, shear stress, and normal stress in both shear-thickening/thinning scenarios. The findings reveal that in both cases, the levels of axial velocity, pressure drop, temperature, shear stress, and normal stress increase as n increases. Notably, the rate of increase is more pronounced in shear-thickening flows compared to shear-thinning flows. A similar trend is observed for the consistency parameter m, where higher values result in amplified effects across all parameters. Additionally, the link between shear rate and viscosity, particularly in the context of shear-thickening/thinning behavior, remains a central focus of this analysis. All of these investigations produced great outcomes that lined up with the predicted physical actions.

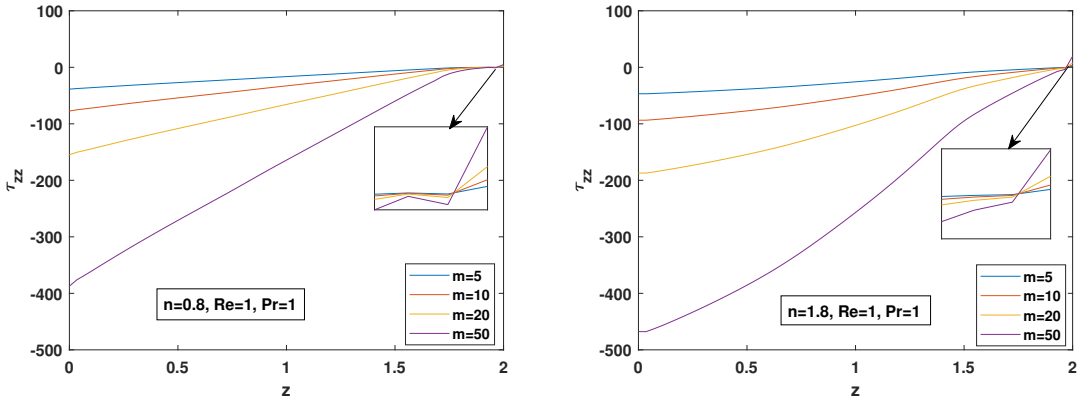

Figure 11: Influence of variation m on axial normal stress.

References

1. Tripathi, S., *Effects of power law fluid characteristics on core-annular flow in a horizontal pipe*, Lect. Notes Mech. Eng. 77–84, (2024).
2. Gooch, J. W. (Ed.), *Power law (Ostwald-de Waele model)*, Encyclopedic Dictionary of Polymers, Springer, New York, NY, 781–781, (2007).
3. Keslerová, R. and Kozel, K., *Numerical modelling of incompressible flows for Newtonian and non-Newtonian fluids*, Math. Comput. Simul. 80(8), 1783–1794, (2010).
4. Siddiqui, A. M., Ahmed, M. and Ghori, Q. K., *Couette and Poiseuille flows for non-Newtonian fluids*, Int. J. Nonlinear Sci. Numer. Simul. 7(1), 15–26, (2006).
5. Jeong, S. W., Leroueil, S. and Locat, J., *Applicability of power law for describing the rheology of soils of different origins and characteristics*, Can. Geotech. J. 46(9), 1011–1023, (2009).
6. Pang, B., Wang, S., Chen, W., Hassan, M. and Lu, H., *Effects of flow behavior index and consistency coefficient on hydrodynamics of power-law fluids and particles in fluidized beds*, Powder Technol. 366, 249–260, (2020).
7. Shareef, A. M. and Al-Muslimawi, A. H., *Numerical investigation of non-Newtonian inelastic flows through conical nozzles*, J. Educ. Pure Sci.-Univ. Thi-Qar 13(4), (2023).
8. Dak, M., Verma, R. C. and Jaaffrey, S. N. A., *Effect of temperature and concentration on rheological properties of Kesar mango juice*, J. Food Eng. 80(4), 1011–1015, (2007).
9. Thohura, S., Molla, M. M. and Sarker, M. M. A., *Numerical simulation of non-Newtonian power-law fluid flow in a lid-driven skewed cavity*, Int. J. Appl. Comput. Math. 5(1), (2019).
10. Al-Haboobi, A. and Al-Muslimawi, A. H., *A new algorithm for solving thermal Newtonian flow in axisymmetric straight channel*, Basrah J. Sci. 41(3), 399–418, (2023).
11. Sharhan, A. and Al-Muslimawi, A., *Inelastic solution for power law fluid with Taylor Galerkin-Pressure Correction finite element method: axisymmetric contraction flows*, J. Appl. Fluid Mech. 16(12), 2411–2423, (2023).
12. Al-Haboobi, A. and Al-Muslimawi, A. H., *Novel algorithm for compressible Newtonian axisymmetric thermal flow*, Int. J. Mod. Phys. C 35(3), (2024).
13. Crank, J. and Nicolson, P., *A practical method for numerical evaluation of solutions of partial differential equations of the heat-conduction type*, Adv. Comput. Math. 6(1), 207–226, (1996).
14. Wu, W. T. and Massoudi, M., *Recent advances in mechanics of non-Newtonian fluids*, Fluids 5(1), Article 10, (2020).
15. Sadiq, N., Jawad, M., Khalid, F., Jahan, S. and Hassan, A. M., *Comparative analysis of non-Newtonian and Newtonian fluid flow with dual slip in the presence of motile microorganisms and nanoparticles*, BioNanoScience 14(2), 1504–1519, (2024).
16. Rohsenow, W. M., Hartnett, J. P., Cho, Y. I. et al., *Handbook of Heat Transfer*, 3rd ed., McGraw-Hill, New York, (1998).
17. Prasad, V. R., Gaffar, S. A., Reddy, E. K. and Bég, O. A., *Numerical study of non-Newtonian Jeffreys fluid from a permeable horizontal isothermal cylinder in non-Darcy porous medium*, J. Braz. Soc. Mech. Sci. Eng. 37(6), 1765–1783, (2015).
18. Sarojamma, G., Sreelakshmi, K. and Animasaun, I. L., *Numerical study of non-linear thermal radiative heat transfer in a non-Darcy chemically reactive Casson fluid flow*, SN Appl. Sci. 1(10), (2019).

19. Chang, A., Sun, H., Vafai, K. and Kosari, E., *Numerical analysis of flow and forced convection heat transfer of non-Newtonian fluid in a pipe based on fractional constitutive model*, Int. J. Numer. Methods Heat Fluid Flow 31(8), 2680–2697, (2021).

20. Ren, X., Xin, Z. and Liu, F., *A non-Newtonian thermal lattice Boltzmann method for simulation of Rayleigh-Bénard convection of power-law fluids*, AIP Adv. 13(11), (2023).

21. Chtaibi, K., Hasnaoui, M., Ben Hamed, H., Dahani, Y. and Amahmid, A., *Numerical simulations of the Lorentz force effect on thermal convection in an inclined square cavity filled with a non-Newtonian fluid*, Lect. Notes Mech. Eng. 196–206, (2024).

22. Hawken, D. M., Tamaddon-Jahromi, H. R., Townsend, P. and Webster, M. F., *A Taylor-Galerkin-based algorithm for viscous incompressible flow*, Int. J. Numer. Methods Fluids 10(3), 327–351, (1990).

23. Tamaddon-Jahromi, H. R., Ding, D., Webster, M. F. and Townsend, P., *A Taylor-Galerkin finite element method for non-Newtonian flows*, Int. J. Numer. Methods Eng. 34(3), 741–757, (1992).

24. Carew, E. O. A., Townsend, P. and Webster, M. F., *A Taylor-Petrov-Galerkin algorithm for viscoelastic flow*, J. Non-Newtonian Fluid Mech. 50(2-3), 253–287, (1993).

25. Ngamaramvaranggul, V. and Webster, M. F., *Computation of free surface flows with a Taylor-Galerkin/pressure-correction algorithm*, Int. J. Numer. Methods Fluids 33(7), 993–1026, (2000).

26. Al-Muslimawi, A. H., *Theoretical and numerical studies of die swell flow*, Korea-Australia Rheol. J. 28(3), 229–236, (2016).

27. Al-Haboobi, A., Al-Juaifri, G. A. and Al-Muslimawi, A. H., *Numerical study of Newtonian laminar flow around circular and square cylinders*, Results Control Optim. 14, (2024).

28. Shapovalov, V. M., *On the applicability of the Ostwald-de Waele model in solving applied problems*, J. Eng. Phys. Thermophys. 90(5), 1213–1218, (2017).

29. Al-Haboobi, A., Fadhel, I. A., Sharhan, A. A. and Al-Muslimawi, A. H., *Computational simulation of compressible Newtonian flow past circular and square bluff bodies*, Ocean Syst. Eng. 14(4), 315–330, (2024).

S. H. Al-Zaidi and A. Al-Haboobi,

Faculty of Computer Sciences & Mathematics,

University of Kufa,

P.O. Box 21, 54001 Al-Najaf, Iraq.

E-mail address: samahh.alzaydi@student.uokufa.edu.iq, anasm.ali@uokufa.edu.iq